Microscopic Theory of Nonlinear Hall Effect in Three-Dimensional Magnetic Systems

Wen-Tao Hou(侯文涛)[1*] and Jiadong Zang(臧佳栋)[2]

[1]*School of Physical Science and Technology, Tiangong University, Tianjin 300387, China*
[2]*Department of Physics and Astronomy, University of New Hampshire, Durham, New Hampshire 03824, USA*

(Received 12 August 2024; accepted manuscript online 10 October 2024)

Nonlinear Hall effect (NLHE) has been detected in various of condensed matter systems. Unlike linear Hall effect, NLHE may exist in physical systems with broken inversion symmetry in crystals. On the other hand, real space spin texture may also break inversion symmetry and result in NLHE. We employ the Feynman diagrammatic technique to calculate non-linear Hall conductivity (NLHC) in three-dimensional magnetic systems. The results connect NLHE with the physical quantity of emergent electrodynamics which originates from the magnetic texture. The leading order contribution of NLHC, χ_{abb}, is proportional to the emergent toroidal moment $\mathcal{T}_a^{\rm e}$, which reflects how the spin textures wind in three dimensions.

DOI: 10.1088/0256-307X/41/11/117502

Plethora of Hall effects have unveiled many exciting physical phenomena in condensed matter physics, such as the quantum spin hall effect, which reveals the non-trivial topological band structures of topological insulators.[1] Unlike linear Hall effects, nonlinear Hall effect (NLHE) would occur in the systems without time reversal symmetry broken.[2,3] Its close connection to non-trivial topology makes NLHE as an useful tool to unlock novel condensed matter systems, such as Weyl semimetals[4,5] and topological insulators.[6,7] Non-linear Hall conductivity (NLHC) χ_{abb} has been measured in layered WTe_2 structures,[8] layered graphene,[9,10] Weyl semimetal $TaIrTe_4$,[11] and topological antiferromagnetic heterostructure.[12] Theoretically, several technical methods have been developed to compute χ_{abb} in real materials, such as Boltzmann transport theory,[13,14] Feynman diagrammatic technique[15–17] and numerical supercell method.[18] It has been revealed that NLHC is associated with the Berry curvature dipole in the reciprocal space.[19–21] The analogy of NLHE in real space can be achieved in magnetic materials hosting topological spin textures. Recent years have witnessed the rising of three-dimensional topological spintronics, whose central topic is to search for the Hopfion,[22,23] a three-dimensional texture resembling a twisted skyrmion tube, in various magnetic systems, such as chiral magnets[24–28] and frustrated magnets.[29,30] The previous research works[31,32] show that χ_{abb} is proportional to the emergent toroidal moment of the Hopfion, expressed as $\mathcal{T}_a^{\rm e} = \frac{1}{2}\int d^3r(\boldsymbol{r}\times\boldsymbol{b})_a$, where $\boldsymbol{b}$ is the emergent magnetic field originating from the local magnetic structures through the semi-classical Boltzmann equation. It is the counterpart of Berry curvature dipole in real space. In our work, a quantum field theoretic approach is employed to derive the NLHC in a three-dimensional magnetic continuous model based on the Feynman diagrammatic technique. We start our calculation from the Hamiltonian of the electrons coupling with local magnetic structure, which is

$$\mathcal{H}_0 = -\frac{\partial_a^2}{2m} - \varepsilon_{\rm F} + V_{\rm imp}(\boldsymbol{r}) - M\boldsymbol{n}(\boldsymbol{r})\cdot\boldsymbol{\sigma}, \tag{1}$$

where m is the mass of electrons, $\varepsilon_{\rm F}$ is Fermi energy and its value is determined by the energy difference from the bottom of an electron band with a quadratic dispersion relationship. Here, we set $\hbar = 1$. $V_{\rm imp}(\boldsymbol{r}) = u_i\delta(\boldsymbol{r}-\boldsymbol{R})$ is the impurity potential. $M = J_{sd}S$ is the rescaled strength of s–d exchange with S being the length of spin field; $\boldsymbol{n}(\boldsymbol{r})$ is a normalized spin vector field, and $\boldsymbol{\sigma} = (\sigma^x,\ \sigma^y,\ \sigma^z)$ are Pauli matrices. Einstein summation convention is employed. With an $SU(2)$ unitary rotation $U^\dagger\boldsymbol{n}\cdot\boldsymbol{\sigma}U \to \sigma^z$ performed, a spin gauge field $\mathcal{A}_a = A_a^i\frac{\sigma}{2}^i = -iU^\dagger\partial_a U$ emerges. Here, the upper indices for Pauli matrices are represented by i, j, k and spatial indices are always at lower position represented by a, b, c, and so on. In this "rotated frame", the spins of electrons can be up and down, which are originally parallel and antiparallel to the local magnetic orientation, respectively, before rotation. The spin field can be decomposed as $\mathcal{A} = \boldsymbol{A}^\perp\frac{\sigma}{2}^\perp + \boldsymbol{A}^z\frac{\sigma^z}{2}$. The diagonal component $\boldsymbol{A}^z$ corresponds to the adiabatic process where no spin flip happens and $\boldsymbol{A}^\perp$ describes the non-adiabatic process since it allows spin flip. There is a relationship between spin gauge field and magnetic structure,

$$(\nabla\times\boldsymbol{A}^z)_a = \varepsilon_{abc}\boldsymbol{n}\cdot(\partial_b\boldsymbol{n}\times\partial_c\boldsymbol{n}), \tag{2}$$

$$(\boldsymbol{A}_b^\perp\times\boldsymbol{A}_c^\perp)^z = \varepsilon_{abc}\boldsymbol{n}\cdot(\partial_b\boldsymbol{n}\times\partial_c\boldsymbol{n}). \tag{3}$$

The right-hand side of Eq. (2) is just the emergent magnetic field b_a which comes from the local magnetic structures. The gauge field $\boldsymbol{A}^z$ is equivalent to the $U(1)$ emergent gauge field $\boldsymbol{a}$ and emergent magnetic field $\boldsymbol{b} = \nabla\times\boldsymbol{a}$

*Corresponding author. Email: houwentao@tiangong.edu.cn
© 2024 Chinese Physical Society and IOP Publishing Ltd

that are responsible for the topological Hall effect observed in many skyrmionic materials.[33] With turning on the external electromagnetic field $\partial_a \to \partial_a - ie\mathcal{A}_{Ea}$, the new Hamiltonian is $\mathcal{H} = \mathcal{H}_0 + \mathcal{H}_i = \mathcal{H}_0 - ej_a\mathcal{A}_{Ea}$. The form with more details is

$$\mathcal{H} = -\frac{1}{2m}\left(\partial_a - iA_a^i\frac{\sigma^i}{2} - ie\mathcal{A}_{Ea}\right)^2 - \varepsilon_{\rm F} + V_{\rm imp} - M\sigma_z, \quad (4)$$

in which $\mathcal{A}_{Ea}$ is the $U(1)$ gauge field corresponding to the external electromagnetic fields and e is the electronic charge. The coupling between electrons and gauge fields can be expressed by the Feynman rules. The ones used in the following calculation are shown in Fig. 1. The dashed tilted lines represent the spin gauge fields. The solid tilted lines represent the external gauge fields which correspond to external electric fields. Different couplings are expressed by different symbols. Through the new form of the Hamiltonian, the diagonal part is treated as non-perturbative one which can be solved as a two-band model.[34] The difference between two bands are the Fermi energies, which are $\mu_\sigma = \varepsilon_{\rm F} + \sigma M$ with $\sigma = \pm 1$ corresponding the electrons with spin "up" and "down". Taking consideration of impurity scattering, the retarded (advanced) Matsubara Green's functions are expressed as

$$G_\sigma^{R(A)}(i\omega_n, k) = (i\omega_n - \varepsilon_{\mathbf{k}} + \mu + \sigma M \pm i\eta_\sigma)^{-1} \quad (5)$$

in which $\varepsilon_k = \frac{k^2}{2m}$ and $\eta_\sigma = \frac{1}{2\tau_\sigma}$. τ_σ is the average scattering time introduced by self-energy calculation which is $\tau_\sigma = \frac{1}{2\pi n_i u_i^2 \nu_\sigma}$. Moreover n_i is the density of impurity and ν_σ is the density-of-states of the σ band electron at the corresponding Fermi surface. In three dimensions, the density of state is $\nu(\varepsilon) = \frac{1}{2\pi^2}\sqrt{\frac{m\varepsilon}{2}}$ and at Fermi surface we have $\nu_\sigma = \frac{1}{2\pi^2}\sqrt{\frac{m\mu_\sigma}{2}}$. The discrete frequency $i\omega_n$ is replaced by a variable $z + i\delta$ for performing analytical continuation. Then the summation over all the possible frequencies of fermions $\sum_n$ will be replaced by $\frac{\beta}{2\pi i}\int dz$, in which $\beta = \frac{1}{k_{\rm B}T}$. Before going to the details of diagrammatic calculation, some assumptions need to be clarified. First we assume $\tau_\uparrow \approx \tau_\downarrow = \tau$. The relationship between $\varepsilon_{\rm F}$ and τ is $\varepsilon_{\rm F}\tau \gg 1$ for a weak disorder situation. The contribution to the conductivities from electrons can be divided into two parts, Fermi surface and Fermi sea. In the weak disorder regime, the contribution from Fermi sea has a factor $1/(\varepsilon_{\rm F}\tau)$ compared to the Fermi surface.[35] Thus, we only consider the contribution from Fermi surface here. The Fermi momentum is $k_{\rm F} = \sqrt{2m\varepsilon_{\rm F}}$ and Fermi velocity is $v_{\rm F} = \sqrt{\frac{2\varepsilon_{\rm F}}{m}}$. The mean free path for the electrons is $l = v_{\rm F}\tau$. We perform the calculation at $ql \ll 1$ regime[36] and local effective field regime $(ql)^2 < M\tau$ in the absence of spin relaxation,[34,37,38] where q is the momentum of spin textures. For a spatially smooth varying magnetic structure, the spin gauge field is treated as perturbation. The requirement of spin gauge field is the amplitude $|\mathcal{A}(q)| \ll k_{\rm F}$. The current is $j_a = -\frac{1}{e}\frac{\delta\mathcal{H}}{\delta A_{Ea}}$. The second order response χ_{abc} in the response relationship has the form

$$j_a = \sigma_{ab}E_b + \chi_{abc}E_bE_c + \cdots. \quad (6)$$

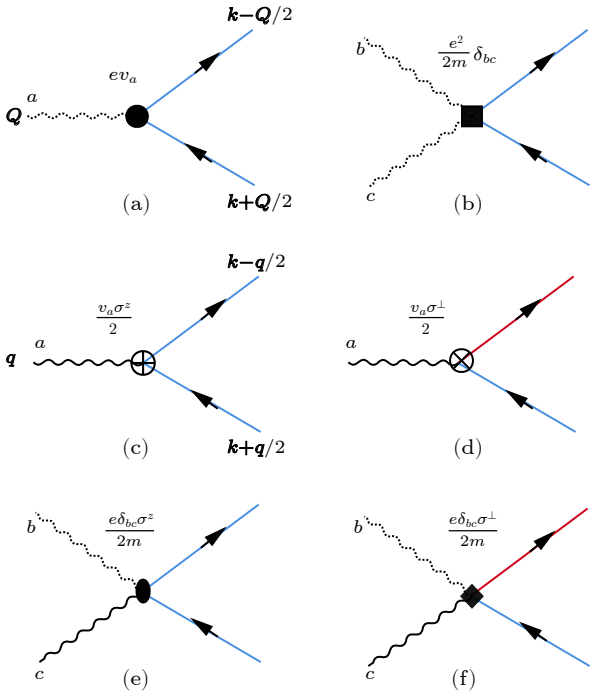

Fig. 1. Feynman Rules.

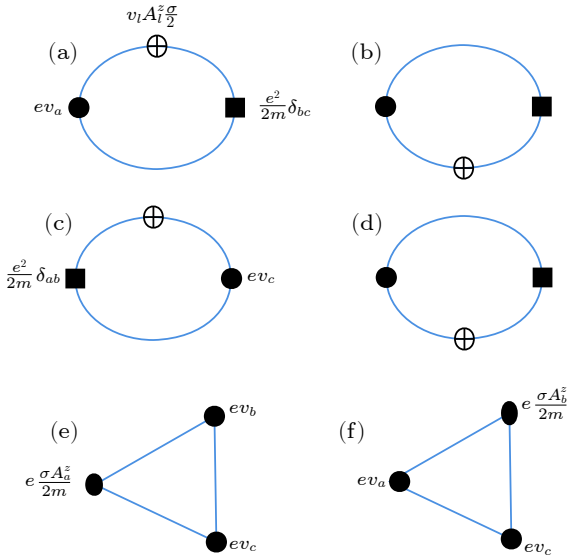

Fig. 2. Diagrams without spin flip that have nonzero leading order contribution.

The first term on the right-hand side of Eq. (6) is the linear response. The definition of second order response χ_{abc} requires that $\chi_{abc} = \chi_{acb}$. When measuring the NLHC, the *ac* input voltage is employed. The external electric field has the form $E_b = i\omega_b A_{Eb}$. The second order response shown by Eq. (6) can be expressed by Feynman diagrams. Inspired by the linear response theory in magnetic systems,[39] in which the leading order contribution to the conductivity is linear in the density of electrons, searching for linear ν_σ terms is the primary task in the process of calculation. The Feynman rules are shown in Fig. 1, where two classes of diagrams contribute to the nonlinear Hall effect, the two-photon and triangle diagrams.

Still inspired by the linear response in magnetic systems, we make a constrain on the combination of the the spin gauge fields will emerge in the results of NLHC. Consequentially, diagrams may contribute to the NLHC can be further categorized, ones without and with spin flip. The leading order with non-zero contribution linear in ν_σ has been shown in Fig. 2. The electron flows are clockwise starting from the left vertex for all diagrams. The contribution $\mathcal{D}_{abb}(\omega, q)$ from Fig. 2(a) is

$$\begin{aligned}\mathcal{D}^{2(a)}_{abb}(\omega, q) = \sum_\sigma \frac{i\sigma e^3}{4\pi}\int dz \int [dk] n'_{\rm F}(z)\frac{k_a k_l A^z_l(q)}{2m^3} \\ \times \Big[G^R_{\sigma,\,k-\frac{q}{2}}(z+\omega)G^R_{\sigma,k+\frac{q}{2}}(z+\omega)G^A_{\sigma,k+\frac{q}{2}}(z) \\ + G^R_{\sigma,k-\frac{q}{2}}(z)G^R_{\sigma,k+\frac{q}{2}}(z)G^A_{\sigma,k+\frac{q}{2}}(z-\omega)\Big],\end{aligned} \tag{7}$$

in which $G^{R(A)}_{\sigma,\,k\pm\frac{q}{2}}(z\pm\omega) = G^{R(A)}_\sigma(z\pm\omega,\, k\pm\frac{q}{2})$, and $n_{\rm F}(z) = \frac{1}{e^{\beta(z-\mu)}+1}$ is the Fermi–Dirac distribution; $n'_{\rm F}(z) \approx -\delta(z)$ is employed for further simplification. With long-wave approximation, the integral can be further approximated by making $q = 0$ in the dominator; $k_a k_l$ can be replaced by $\frac{1}{d}\delta_{al}k^2$ since the electron band is isotropic and the integral dimension is $d = 3$. As a result, we have

$$\begin{aligned}\mathcal{D}^{2(a)}_{abb}(\omega, q) \approx \frac{e^3}{4\pi i m^2}\sum_\sigma \int [dk]\frac{k^2}{3m}A^z_a(q) \\ \times \Big[G^R_{\sigma,\,k}(\omega)G^R_{\sigma,k}(\omega)G^A_{\sigma,k}(0) \\ + G^R_{\sigma,k}(0)G^R_{\sigma,k}(0)G^A_{\sigma,k}(-\omega)\Big],\end{aligned} \tag{8}$$

and similarly

$$\begin{aligned}\mathcal{D}^{2(b)}_{abb}(\omega, q) \approx \frac{e^3}{4\pi i m^2}\sum_\sigma \int [dk]\frac{k^2}{3m}A^z_a(q) \\ \times \Big[G^R_{\sigma,\,k}(\omega)G^A_{\sigma,k}(0)G^A_{\sigma,k}(0) \\ + G^R_{\sigma,k}(0)G^A_{\sigma,k}(-\omega)G^A_{\sigma,k}(-\omega)\Big].\end{aligned} \tag{9}$$

Then the integral $\int[dk] = \int \nu(\varepsilon)d\varepsilon$ is used for the integral and $\nu(\varepsilon) = \frac{1}{2\pi^2}\sqrt{\frac{m\varepsilon}{2}}$. As a consequence, the density of states around fermi surface is $\nu_\sigma = \frac{1}{2\pi^2}\sqrt{\frac{m\mu_\sigma}{2}}$. Then the contribution to the nonlinear Hall conductance under *dc* limit is

$$\begin{aligned}&\Xi^{2(a)+(b)}_{abb}(q) \\ &= \lim_{\omega\to 0}\frac{\mathcal{D}^{2(a)+(b)}_{abb}(\omega, q) - \mathcal{D}^{2(a)+(b)}_{abb}(0, q)}{\omega} \\ &= \frac{\partial \mathcal{D}^{2(a)+(b)}_{abb}(\omega, q)}{\partial\omega}\Big|_{\omega=0} \approx \frac{e^3\tau^2 A^z_a(q)}{2m^2}\sum_\sigma \sigma\nu_\sigma.\end{aligned} \tag{10}$$

The diagrams in Figs. 2(c) and 2(d) contribute to NLHC $\chi_{aba} = \chi_{aab}$ by

$$\Xi^{2(c)+(d)}_{aba}(q) = \Xi^{2(c)+(d)}_{aab}(q) \approx \frac{e^3\tau^2 A^z_a(q)}{2m^2}\sum_\sigma \sigma\nu_\sigma. \tag{11}$$

Triangle diagram contribution to χ_{abb} is shown in Figs. 2(e) and 2(f), corresponding to χ_{bab} and χ_{bba}. The contribution to the NLHC is

$$\Xi^{2(e)}_{abb}(q) = \Xi^{2(f)}_{bba}(q) = \Xi^{2(f)}_{bab}(q) \approx \frac{e^3\tau^2 A^z_a(q)}{2m^2}\sum_\sigma \sigma\nu_\sigma. \tag{12}$$

The diagrams with spin flip contribution to NLHC is shown in Fig. 3. The contribution to the *dc* nonlinear Hall conductance is

$$\begin{aligned}&\Xi^{3(a)+(b)}_{abb}(Q = q' - q) \\ &\approx \frac{e^3\tau^2}{m^2}\frac{1}{4M^2\tau^2+1}\Big(\boldsymbol{A}^\perp_a(q') \times i\frac{\partial}{\partial q_l}\boldsymbol{A}^\perp_l(-q)\Big)^z \sum_\sigma \sigma\nu_\sigma.\end{aligned} \tag{13}$$

The details of calculation are shown in Section Ⅱ(B) of the Supplemental Materials. The diagrams with exchange of the left and right vertices in Fig. 3 will give the contribution expressed as

$$\Xi^{3(c)+(d)}_{bab}(Q) = \Xi^{3(c)+(d)}_{bba}(Q) = \Xi^{3(a)+(b)}_{abb}(Q). \tag{14}$$

It is the same as the cases without spin flip.

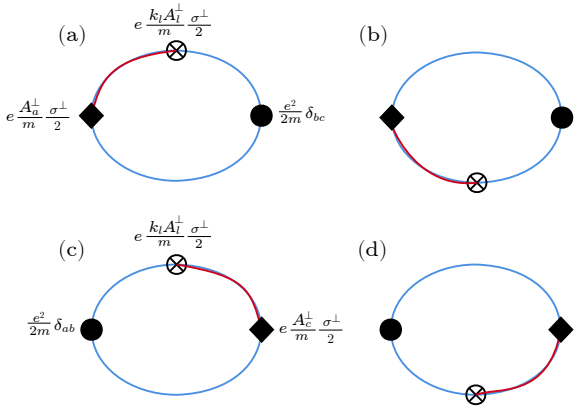

Fig. 3. Diagrams with spin flip that have nonzero leading order contribution.

Previous research works predicted that NLHC χ_{abb} is proportional to the emergent toroidal moment which is $\mathcal{T}^{\rm e}_a = \frac{1}{2}\int[dr](\boldsymbol{r}\times\boldsymbol{B}^z(r))_a$.[40,41] Actually a general expression for the gauge field $\boldsymbol{A}^z(r)$ can be expressed as

$$\boldsymbol{A}^z(r) = \frac{1}{2}\boldsymbol{B}^z(r)\times\boldsymbol{r} + \nabla\Lambda(r) \tag{15}$$

up to a gauge transformation of the symmetric gauge. In long-wave approximation $q \to 0$, the gauge field in the reciprocal space $A^z_a(q) = \int[dr]A^z_a(r)e^{i\boldsymbol{q}\cdot\boldsymbol{r}}$ is given by

$$A^z_a(q=0) = \int[dr]A^z_a(r) = -\mathcal{T}^{\rm e}_a. \tag{16}$$

In real space, the density of toroidal moment can be expressed as

$$\frac{1}{2}(\boldsymbol{r}\times\boldsymbol{B}^z(r))_a = r_b(\boldsymbol{A}^\perp_a\times\boldsymbol{A}^\perp_b)^z. \tag{17}$$

In local effective regime, we have

$$\begin{aligned}\mathcal{T}_a^{\rm e} &= \int [dr]\frac{1}{2}(\boldsymbol{r}\times\boldsymbol{B}^z(r))_a \\ &= \int [dr][dq][dq']r_b(\boldsymbol{A}_a^{\perp}(q')\times\boldsymbol{A}_b^{\perp}(-q))^z e^{-i(\boldsymbol{q}'-\boldsymbol{q})\cdot\boldsymbol{r}} \\ &= \int [dr][dq][dq'](\boldsymbol{A}_a^{\perp}(q')\times\boldsymbol{A}_b^{\perp}(-q))^z \frac{\partial}{i\partial q_b}e^{-i(\boldsymbol{q}'-\boldsymbol{q})\cdot\boldsymbol{r}} \\ &= \int [dq]\boldsymbol{A}_a^{\perp}(q)\times i\frac{\partial}{\partial q_b}\boldsymbol{A}_b^{\perp}(-q). \end{aligned} \tag{18}$$

A partial integral is performed in Eq. (18). In the nonlocal effective field case, the real space expression of Eq. (13) would have another form.[34,38] Then in the long-wave approximation, the toroidal moment can be further simplified to

$$\begin{aligned}\mathcal{T}_a^{\rm e} &\approx \Big(\int [dq]\Big)\lim_{q\to 0}\Big(\boldsymbol{A}_a^{\perp}(q)\times i\frac{\partial}{\partial q_b}\boldsymbol{A}_b^{\perp}(-q)\Big)^z \\ &= \lim_{q\to 0}\Big[\boldsymbol{A}_a^{\perp}(q)\times i\frac{\partial}{\partial q_b}\boldsymbol{A}_b^{\perp}(-q)\Big]^z. \end{aligned} \tag{19}$$

To summarize, the nonlinear Hall conductivity is

$$\begin{aligned}\chi_{abb}^{(in)} &= \frac{1}{4}[\Xi_{abb}^{1(a)+(b)}(0)+\Xi_{abb}^{1(c)}(0)+\Xi_{abb}^{2(a)+(b)}(0)] \\ &\approx -\frac{e^3\tau^2}{4m^2}\Big(1-\frac{1}{4M^2\tau^2+1}\Big)\mathcal{T}_a^{\rm e}\sum_{\sigma}\sigma\nu_{\sigma}. \end{aligned} \tag{20}$$

The factor $\frac{1}{4}$ comes from the *dc* limit approach which is shown in Section I of the Supplemental Materials. The relationships between the nonlinear conductivities are

$$\frac{\chi_{aaa}^{(in)}}{2} = \chi_{abb}^{(in)} = \chi_{bab}^{(in)} = \chi_{bba}^{(in)}, \tag{21}$$

in which $a\neq b$. The difference between χ_{abb} and $\chi_{acc}(b\neq c)$ for an anisotropic system has not emerged in the leading order contribution. Unlike linear response, the leading order of nonlinear Hall conductivities at one-loop level are dependent of relaxation time τ. Beyond one-loop level, the corrections[34] would be included. They can be shown by the ladder correction which are shown in Fig. 4. Figure 4(a) describes correction to the spin-flip processing involved by impurity scattering, which is expressed as $\Pi_{\bar{\sigma}\sigma}(q) = \frac{n_i u_i^2(1+2i\sigma M)}{(Dq^2+2i\sigma M-i\omega+\tau_s^{-1})\tau}$. Here τ_s is the average spin relaxation time.[42] The contribution can be neglected in the absence of spin relaxation assumption, which is $\tau/\tau_s \gg 1$. This means that the spin flip is too fast to encounter the impurity scattering. Figure 4(b) contributes to vertex correction with a factor of $\frac{Dq^2}{Dq^2-i\omega}$, where $D=\frac{1}{3}v_{\rm F}^2\tau$ is a relaxation constant.[34,36] It has no contribution after performing *dc* limit ($\omega\to 0$) and long-wave approximation ($q\to 0$) sequentially.

Compared to the work using Boltzmann transport,[32] our quantum field theoretic approach gives an additional $M\tau$-dependent result. Actually, strong coupling ($M\tau \ll 1$) was employed in Ref. [32], so that both results are consistent. Our result is valid for both weak coupling ($M\tau<1$) and strong coupling ($M\tau>1$) regimes through the long-wave approximation and local effective field assumption. On the other hand, in the weak coupling limit $M\tau\to 0$, which is equivalent to the situation, there is no coupling between electrons and local magnetic textures, the electrons turn to be an isotropic gas; χ_{abb} thus turns to be zero, which is consistent with the result of isotropic electron gas systems.

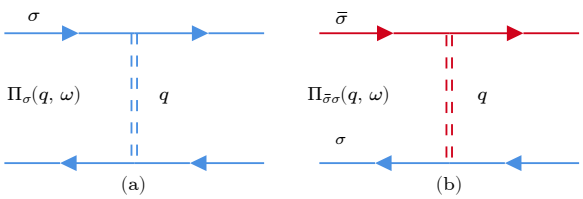

Fig. 4. Ladder corrections.

In three dimensions, if the magnetic structure gives rise to an emergent magnetic field as $\boldsymbol{b}=b_0e^{-\alpha\rho}\hat{\theta}$ along the azimuth direction in cylindrical coordinates, where b_0 and $\alpha(\alpha>0)$ are constants and $\rho=\sqrt{x^2+y^2}$, the toroidal moment is given by

$$\boldsymbol{T}^{\rm e} = \int [dr]\frac{1}{2}\boldsymbol{r}\times\boldsymbol{b} = \frac{\pi b_0}{\alpha^2}\hat{z}. \tag{22}$$

This toroidal moment leads to a nonzero NLHC χ_{abb} in the presence of impurity scattering. A specific example is the magnetic Hopfion. A Hopfion with the Hopf number $h=1$ can be parameterized as

$$\boldsymbol{n}(r) = \hat{z}+\frac{\sin 2\eta(r)}{r}(x,\,y,\,0)-\frac{2\sin^2\eta(r)}{r^2}(-yz,\,xz,\,x^2+y^2), \tag{23}$$

in which $r=\sqrt{x^2+y^2+z^2}$, and $\eta(r)$ is an arbitrary monotonic function with constraints $\eta(0)=0$ and $\eta(\infty)=\pi$.[26] The emergent magnetic field can be calculated by $b_a=\varepsilon_{abc}\boldsymbol{n}\cdot(\partial_b\boldsymbol{n}\times\partial_c\boldsymbol{n})$. Then the emergent toroidal moment of the Hopfion is

$$\boldsymbol{T}^{\rm e} = \int [dr]\frac{1}{2}\boldsymbol{r}\times\boldsymbol{b} = \frac{2}{3}\int [dr]\sin^2\eta(r)\eta'(r)\hat{z}. \tag{24}$$

A proper choice of $\eta(r)$ will make the toroidal moment nonzero and finite.[43]

The origin of nonzero NLHC is diverse. For instance, momentum space Berry curvature dipole dominates the intrinsic NLHE. Previous works have discussed this factor in various of condensed matter systems.[19,20,44,45] Beyond intrinsic NLHE, a recent study on CuAsMn offers another mechanism for NLHE.[46] From a symmetry perspective, hidden spin polarization locally breaks the inversion symmetry in real space. When combined with the asymmetry of electron band structures, it leads to the observable NLHC. Our result presents another mechanism. The existence of nonzero emergent toroidal moment breaks both inversion and time reversal symmetries in real space which results in a nonzero NLHC. More generally, nonzero NLHC χ_{abb} would emerge in a variety of multi-q magnetic states that have nonzero toroidal moments.

Acknowledgements. W. T. Hou was supported by the Startup Foundation in Tiangong University (Grant No. 63010201/52010399). J. Zang was supported by the Office of Basic Energy Sciences, Division of Materials Sciences and Engineering, U.S. Department of Energy (Grant

No. DE-SC0020221). W. T. Hou would like to thank Professor Yi Liao and Dr. Xiao-Dong Ma for beneficial discussion about Feynman diagrammatic techniques. W. T. Hou and J. Zang would like to thank Dr. Kazuki Nakazawa for delighted discussion on linear response theory in magnetic systems, and also thank Dr. Yizhou Liu for Boltzmann transport theory. W. T. Hou would like to thank Professor Wenhong Wang and Dr. Jie Chen for discussion on experiments of electronic conductivities in magnetic systems.

References

[1] Bernevig B A and Zhang S C 2006 *Phys. Rev. Lett.* **96** 106802
[2] Du Z Z, Wang C M, Li S, Lu H Z, and Xie X C 2019 *Nat. Commun.* **10** 3047
[3] Ortix C 2021 *Adv. Quantum Technol.* **4** 2100056
[4] Li R H, Heinonen O G, Burkov A A, and Zhang S S L 2021 *Phys. Rev. B* **103** 045105
[5] Ovalle D G, Pezo A, and Manchon A 2022 *Phys. Rev. B* **106** 214435
[6] Yasuda K, Tsukazaki A, Yoshimi R, Kondou K, Takahashi K S, Otani Y *et al.* 2017 *Phys. Rev. Lett.* **119** 137204
[7] Rao W, Zhou Y L, Wu Y J, Duan H J, Deng M X, and Wang R Q 2021 *Phys. Rev. B* **103** 155415
[8] Ma Q, Xu S Y, Shen H T, MacNeill D, Fatemi V, Chang T R *et al.* 2019 *Nature* **565** 337
[9] Zhang C P, Xiao J W, Zhou B T, Hu J X, Xie Y M, Yan B H *et al.* 2022 *Phys. Rev. B* **106** L041111
[10] Duan J X, Jian Y, Gao Y, Peng H M, Zhong J r, Feng Q *et al.* 2022 *Phys. Rev. Lett.* **129** 186801
[11] Kumar D, Hsu C H, Sharma R, Chang T R, Yu P, Wang J *et al.* 2021 *Nat. Nanotechnol.* **16** 421
[12] Gao A Y, Liu Y F, Qiu J X, Ghosh B, Trevisan T V, Onishi Y *et al.* 2023 *Science* **381** 181
[13] Nandy S and Sodemann I 2019 *Phys. Rev. B* **100** 195117
[14] Xiao C, Du Z Z, and Niu Q 2019 *Phys. Rev. B* **100** 165422
[15] Parker D E, Morimoto T, Orenstein J, and Moore J E 2019 *Phys. Rev. B* **99** 045121
[16] Du Z Z, Wang C M, Sun H P, Lu H Z, and Xie X C 2021 *Nat. Commun.* **12** 5038
[17] Michishita Y and Peters R 2021 *Phys. Rev. B* **103** 195133
[18] Chen R, Du Z Z, Sun H P, Lu H Z, and Xie X C 2024 *Phys. Rev. B* **110** L081301
[19] Gao Y, Yang S A, and Niu Q 2014 *Phys. Rev. Lett.* **112** 166601
[20] Sodemann I and Fu L 2015 *Phys. Rev. Lett.* **115** 216806
[21] Lai S, Liu H Y, Zhang Z W, Zhao J Z, Feng X L, Wang N Z *et al.* 2021 *Nat. Nanotechnol.* **16** 869
[22] Kent N, Reynolds N, Raftrey D, Campbell I T, Virasawmy S, Dhuey S *et al.* 2021 *Nat. Commun.* **12** 1562
[23] Yu X, Liu Y, Iakoubovskii K V, Nakajima K, Kanazawa N, Nagaosa N, and Tokura Y 2023 *Adv. Mater.* **35** 2210646
[24] Liu Y, Lake R K, and Zang J 2018 *Phys. Rev. B* **98** 174437
[25] Sutcliffe P 2018 *J. Phys. A* **51** 375401
[26] Liu Y Z, Hou W T, Han X F, and Zang J D 2020 *Phys. Rev. Lett.* **124** 127204
[27] Khodzhaev Z and Turgut E 2022 *J. Phys.: Condens. Matter* **34** 225805
[28] Zheng F S, Kiselev N S, Rybakov F N, Yang L Y, Shi W, Blügel S *et al.* 2023 *Nature* **623** 718
[29] Sutcliffe P 2017 *Phys. Rev. Lett.* **118** 247203
[30] Naya C, Schubring D, Shifman M, and Wang Z 2022 *Phys. Rev. B* **106** 094434
[31] Göbel B, Akosa C A, Tatara G, and Mertig I 2020 *Phys. Rev. Res.* **2** 013315
[32] Liu Y, Watanabe H, and Nagaosa N 2022 *Phys. Rev. Lett.* **129** 267201
[33] Schulz T, Ritz R, Bauer A, Halder M, Wagner M, Franz C *et al.* 2012 *Nat. Phys.* **8** 301
[34] Nakazawa K, Bibes M, and Kohno H 2018 *J. Phys. Soc. Jpn.* **87** 033705
[35] Mahan G D 2013 *Many-Particle Physics* (Springer Science & Business Media)
[36] Coleman P 2015 *Introduction to Many-Body Physics* (Cambridge University Press)
[37] Onoda M, Tatara G, and Nagaosa N 2004 *J. Phys. Soc. Jpn.* **73** 2624
[38] Nakazawa K and Kohno H 2019 *Phys. Rev. B* **99** 174425
[39] Bruno P, Dugaev V K, and Taillefumier M 2004 *Phys. Rev. Lett.* **93** 096806
[40] Dubovik V M and Tugushev V V 1990 *Phys. Rep.* **187** 145
[41] Spaldin N A, Fiebig M, and Mostovoy M 2008 *J. Phys.: Condens. Matter* **20** 434203
[42] D'yakonov M I and Perel V I 1971 *Sov. J. Exp. Theor. Phys.* **33** 1053
[43] Pershoguba S S, Andreoli D, and Zang J 2021 *Phys. Rev. B* **104** 075102
[44] Liu H, Zhao J, Huang Y X, Wu W, Sheng X L, Xiao C, and Yang S A 2021 *Phys. Rev. Lett.* **127** 277202
[45] Wang C, Gao Y, and Xiao D 2021 *Phys. Rev. Lett.* **127** 277201
[46] Chen W, Gu M, Li J, Wang P, and Liu Q 2022 *Phys. Rev. Lett.* **129** 276601